Multilayer injection molding. Part 2: Particle tracking in reactive molding

*G. W. M. Peters, P. J. L. van der Velden, H. E. H. Meijer**
Centre for Polymers and Composites, Eindhoven University of Technology, Netherlands
P. Schoone
Philips CFT, Eindhoven, Netherlands

Multilayer Injection Moulding

Part 2: Particle tracking in reactive moulding

The modelling of multilayer reactive injection moulding is studied. After presenting the equations describing the process, two important aspects are dealt with in more detail. These are particle tracking and the modelling of the flow front. First results demonstrate the possibilities of the modelling and show satisfactory agreement between predictions of numerical simulations and experimental results, concerning particle tracking in the whole flow domain and the break-through of layers in sequential two component moulding.

1 Introduction

Multilayer injection moulding is the extension of the standard injection moulding technology to allow for more components that can be simultaneously or sequentially (co-)injected. For flexibility in combining different materials, at least three components are needed [1]. Maintaining the versatility in complex geometries, which allows for the fabrication of highly integrated parts, requires the possibility of predicting sequence and configuration of the materials that should be forced into the mould in order to realize a specific configuration in the product. To be able to make such predictions, computer programs are needed for the numerical simulation of 3-D transient non-isothermal flow problems of non-Newtonian, sometimes even reactive, fluids. Key parts of such a computer code are the methods chosen to deal with particle tracking and flow front computation. Particle tracking provides the deformation history of every fluid element that enters the mould [1, 2]. The flow front model determines the final position of all particles close to the wall, including the prediction of layer break-through; that is if the secondly injected material reaches the outside of the product via the fountain flow at the front. The surroundings of the flow front is called the flow front domain. The rest of the domain is called the main flow.

Most recent computer programs developed for the numerical simulation of injection moulding are restricted to cavities for thin walled, weakly curved, but geometrical complex products [3 to 7]. Based on this limitation a $2\frac{1}{2}$-D approach is used, solving the pressure problem with finite elements in 2-D and the temperature and velocity field with finite differences in 3-D. A particle tracking algorithm and a more realistic flow front model have been incorporated in existing $2\frac{1}{2}$-D computer codes; INJECT-3 [2, 3] (used in this paper) and VIp, the EUT program [4].

2 Modelling the injection moulding process

As stated above, in modelling the injection moulding process usually the restriction is made by considering only narrow, weakly curved channels and, therefore, the lubrication approximation can be employed [7]. The material is described as a compressible, heat conducting, reactive, viscous fluid. After substitution of the usual simplifications and the constitutive equations in the balance equations, the following system of equations is obtained (see, e.g. [4]):

Mass: $$\vec{\nabla}^* \cdot \vec{v}^* + \frac{\partial v_n}{\partial x_n} = \frac{\dot{\varrho}}{\varrho}, \tag{1}$$

Momentum: $$\vec{\nabla}^* p = \frac{\partial}{\partial x_n}\left(\eta \frac{\partial \vec{v}^*}{\partial x_n}\right), \quad \frac{\partial p}{\partial x_n} = 0, \tag{2}$$

Energy: $$\varrho c_p \dot{T} = \frac{\partial}{\partial x_n}\left(\lambda \frac{\partial T}{\partial x_n}\right) + \eta\dot{\gamma}^2 - \frac{T}{\varrho}\left(\frac{\partial \varrho}{\partial T}\right)_p \dot{p} + \varrho h_r R_c, \tag{3}$$

Moles: $$\dot{C} = -R_c, \tag{4}$$

Identity: $$\dot{\xi} = 0. \tag{5}$$

Use is made of the decomposition of any arbitrary vector $\vec{a}$ into a component $\vec{a}^*$ (parallel to the midplane) and a component a_n in the $\vec{n}_3$ direction (the direction normal to the midplane):

$$\vec{a} = \vec{a}^* + a_n \vec{n}_3. \tag{6}$$

The conservation of identity (5) expresses that, for a material particle, a once given set of labels ξ does not change. This unique set, which represents the identity of a particle, is assigned to a particle when it enters the flow domain. In the most general case, a 3-D flow in arbitrary shaped cavities, a set of labels consisting of the coordinates of the place where a particle enters the flow domain and the time this occurs is sufficient to identify each particle uniquely.

The material functions for the heat capacity c_p, the density ϱ and the viscosity η have to be specified. For many

* Mail address: Prof. Dr. H. E. H. Meijer, Centre for Polymers and Composites, Eindhoven University of Technology, P.O. Box 513, 5600 MB Eindhoven, Netherlands.

materials these functions can be found in literature. For reactive materials, however, they still have to be determined in most cases. Examples of such measurements can be found in [6, 8].

The set of equations (1 to 5), as given above, consists of ten (1, 3, 1, 1, 4) instationary, non-linear, coupled equations, in which ten unknown variables p, T, $\dot{\gamma}^*$, v_n, C and ξ (1, 1, 2, 1, 1, 4) appear. These equations must be solved iteratively.

The so-called pressure problem is derived by elimination of the velocity from Eqs. (1) and (2) through integration over the thickness, yielding an equation with the pressure as the only unknown variable [6, 9]. An approximate solution for this equation is obtained on the domain of the midplane for $0 < t < t_{fill}$ by employing the finite element method. After the pressure is solved, the velocities are obtained from the momentum equation. Next, an approximate solution for the temperature field is obtained by means of the finite difference method. In every node of the finite element mesh, used for the pressure equation, a gridline in the $\vec{n}_3$ direction is defined over the local height of the channel. An implicit Euler scheme is used. The convective term of $\varrho c_p \dot{T}$ is discretized with a first order backward scheme. Derivatives with respect to the $\vec{n}_3$ direction are discretized with a central difference scheme. Finally, a triangular matrix equation results which is easily solved node by node [10].

The equations for conversion and identity, which are pure convective equations (Damkohler II $\gg$ 1, diffusion of reactants is negligible in the equation for conversion), are solved in an identical way. Notice that the boundary values for these variables are only prescribed on the inflow part of the channel. It is known that these equations must be treated with special care because many numerical solution schemes introduce too much numerical diffusion, resulting in smearing out of strong gradients [11, 12].

Front propagation is described in detail in [5]. The front intersects with element edges of the fixed finite elements. Temporary nodes are created at these intersections and, within elements with intersected edges, temporary elements are created between fixed and temporary nodes. The complete flow front consists of a number of connected edges of temporary elements. The local front velocity is taken equal to the average velocity in the connected temporary element.

The most important advantage of the mixed use of the finite element/finite difference method is the ability to deal with complex geometries in still reasonable computation time.

3 Flow front modelling

Material near the midplane of the cavity in the bulk of the fluid flows faster than the front. As material from the central region reaches the front, its velocity decreases and a velocity component towards the wall is introduced. The flow becomes of a spreading nature which is called fountain flow (Fig. 1). This subdomain, where the flow is much more complex than in the rest of the domain, constitutes only a small portion of the total flow domain (except at the beginning of filling). The dimensions are in the order of the local height of the cavity.

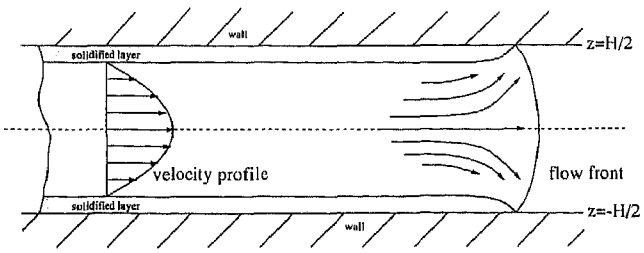

Fig. 1. Fountain flow in the flow front domain

Simple models for the flow front domain can be used when only temperature fields in non-reactive materials, or reactive processing with high Graetz and low Damköhler IV numbers are considered [3, 5, 13, 14]. However, in the case of particle tracking or in the more general case of reactive materials more sophisticated models are needed [11, 15, 16]. An accurate model for the flow front is of decisive importance for the correct prediction of the breakthrough of wall layers by core material and incomplete mouldfilling due to premature gelation. However, application of an analytical model is necessary as CPU time would otherwise increase unacceptably.

The 2D quasi-analytical model as proposed by Bhattacharji and Savic resp. Castro and Macosko [11, 15] is adapted here for the 3D flow (see next section). The most important assumptions underlying this model are:

- the flow front is flat (contact angle = 90°),
- the flow is quasi-stationary,
- the viscosity is constant (no influence of temperature or conversion),
- no slip at the wall occurs, except at the moving contact line,
- inertia can be neglected.

Experimental work and detailed numerical simulations of the fountain flow have shown that the introduction of a more realistic flow front shape, the nonisothermal effects and even large differences in rheological properties, i.e. Newtonian, shear thinning and/or viscoelastic fluids [11, 12, 17] do not alter the overall kinematics significantly. The reason for this is that the global kinematics are largely determined by the conservation of mass rather than the conservation of momentum. Here, only the final result, a fourth order approximation, is given in terms of the velocity field with respect to an observer moving along with the front [15] (see Fig. 2):

$$\frac{v_x}{\bar{v}_x} = -(0.5 - 6z^2/H^2) \times [1 - 1.45 \exp(-5x/H) \sin(0.76 + 2x/H)] - 0.53(1 - 80z^4/H^4) \exp(-5x/H) \sin(2x/H), \quad (7)$$

$$\frac{v_z}{\bar{v}_x} = z/H\,(1 - 4z^2/H^2)[3.63 \exp(-5x/H) \sin(0.76 + 2x/H) - 1.45 \exp(-5x/H) \cos(0.76 + 2x/H)] - 2z/H\,(1 - 16z^4/H^4)[1.32 \exp(-5x/H) \sin(2x/H) - 0.53 \exp(-5x/H) \cos(2x/H)], \quad (8)$$

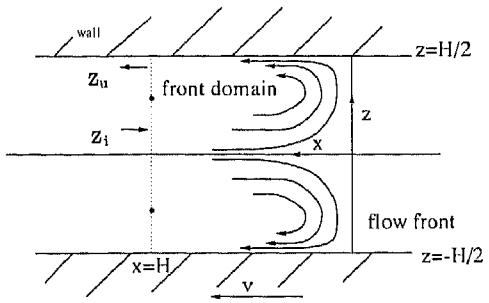

Fig. 2. Flow front domain definitions with respect to the moving front; a material particle entering the domain at z_l leaves at z_u; the folding points (see text) are indicated with a " • "

where $\bar{v}_x$ is the average velocity in x-direction, the front velocity. This approximation causes a transition from no slip to slip between $0 \leq x \leq 0.1H$. The length of the flow front domain is taken equal the local thickness of the mould. At this position, the velocity profile is almost parabolic, which corresponds with a pressure driven flow of a Newtonian fluid between two parallel plates. On the interface between the flow front domain and the main domain at $z = \pm H/2\sqrt{3}$ (see Fig. 2, that shows, in contrast to Fig. 1, the streamlines relative to the moving front), the x-component of the velocity is zero. These points are called the folding points. Material between these points flows from the main flow domain into the flow front domain. Material between the folding points and the wall flows the opposite direction.

Particle tracking has to be done only once for the flow front domain. The results are stored in a dimensionless form. Dimensions are scaled with the half height H/2 of the cavity. The dimensionless residence time is defined as:

$$\bar{t}_r = \frac{t_r \bar{v}_x}{H/2}, \tag{9}$$

where $\bar{v}_x$ is the front velocity. The residence time of a particle in the flow front domain as a function of the position where a particle leaves the flow front domain, is given in Fig. 3. It can be described sufficiently accurately with a sixth order polynomial.

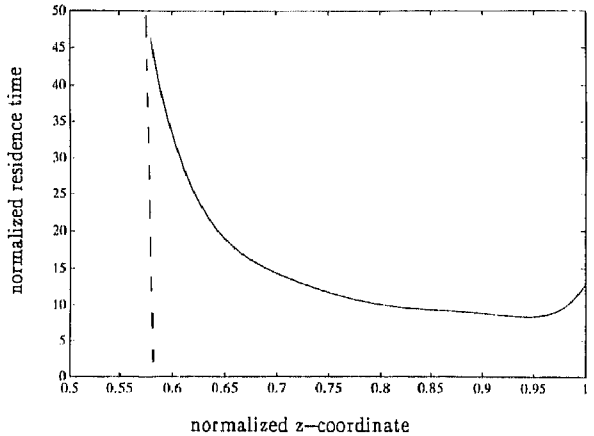

Fig. 3. Normalized residence time ($\bar{t}_r = t_r \bar{v}_x / (H/2)$) as a function of normalized position ($\bar{z}_u = z_u / (H/2)$) where a particle leaves the flow front domain; the dashed line indicates the position of the folding point (see text)

4 Application of the front model with particle tracking

4.1 Reduction from a 3D to a local 2D problem

Flow in the mould is essentially 3D and transient. The question is how to incorporate the (stationary 2D stationary) flow front model. A cross-section at an arbitrary position at the front in a plane spanned by the normal vector $\vec{n}$ (in the midplane, pointing outwards from the domain, see Fig. 4) and the local base vector $\vec{n}_3$, is considered as a 2D front flow domain. The dimensions of this domain are $H \times H$. It is assumed that this domain moves along a curved surface that can be described by a curved line through the midplane of the cavity and the local base vector $\vec{n}_3$. This assumption is supported by the knowledge that the pressure gradient tangential to the front, in the close surrounding of the front, is zero:

$$\frac{\partial p}{\partial \vec{t}} = 0. \tag{10}$$

The flow in the cross-sections as defined above is considered quasi-stationary.

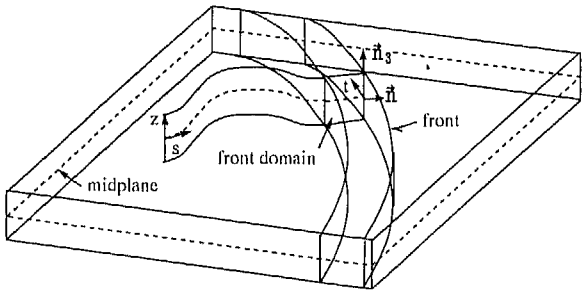

Fig. 4. Definition of the 2D flow front domain in a 3D mould

The approximated pressure field is linear within an element. The velocity $v^*(z)$ is a linear function of the pressure gradient. Thus, the velocity profile $v^*(z)$ is the same everywhere within an element. When a gridline is passed by the front flow domain, the average velocity $\bar{v}^*$ of the corresponding elements is assigned to that gridline as the velocity with which the flow front domain passed. Upstream, upon crossing an element side, the curved plane along which the flow front domain has passed this element must be reconstructed. An approximation thereof is represented by the plane spanned by the interpolated value of the flow front domain velocities from the gridlines corresponding to the crossed element side, and $\vec{n}_3$ (see Fig. 5). Particle tracking is performed along these approximated planes.

From the time a gridline is passed by the flow front domain, it is part of the main flow domain. However, before such a line fits in the algorithm that is used in the main flow, values of the variables considered should be initialized on this line. For that purpose gridpoints between the folding points, which are fed from material from the main flow domain, and gridpoints between a folding point and a wall, which are fed by material from the front flow domain, are considered separately.

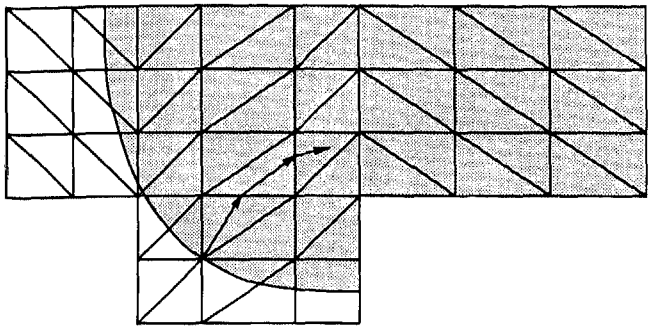

Fig. 5. Reconstruction of the flow front domain flow plane. The arrows indicate the approximate flow plane

4.2 Gridpoints between folding points and the wall

Now that the problem is reduced to a 2D problem in the curved plane along which the flow domaim moves (see Figs. 4 and 5), it is possible, by means of the flow front model, to determine the position $\tilde{z}_i$ and time $t - t_r$ (t_r is the flow front domain residence time) of entering the flow front domain, for a given particle leaving the front domain at position $\tilde{z}_u$ (see Fig. 2) at time t. The set of labels $\underset{\sim}{\xi}$ corresponding to the material particle under consideration follows from

$$\underset{\sim}{\xi}(\tilde{x}_u,t) = \underset{\sim}{\xi}(\tilde{x}_i,t - t_r). \tag{11}$$

4.3 Gridpoints between the folding points

Material particles in these gridpoints originate from the main flow domain. Upstream information should be obtained from upstream gridpoints. The procedure is here elucidated for the 2D case. However, it can directly be applied in the 3D case as may be clear from the foregoing.

The time for a particle to travel from one gridpoint to the other is given by:

$$\Delta t'(z) = \frac{\|\Delta\tilde{x}\|}{v(z)}, \tag{12}$$

where $\|\Delta\tilde{x}\|$ is the distance between the gridlines. The set of labels $\underset{\sim}{\xi}$ corresponding to the material particle under consideration is given by:

$$\underset{\sim}{\xi}(\tilde{x},t) = \underset{\sim}{\xi}(\tilde{x} - \Delta\tilde{x},t - \Delta t'). \tag{13}$$

The values of $\underset{\sim}{\xi}$ at position $\tilde{x} - \Delta\tilde{x}$ on time level $t - \Delta t'$ are not known. However at this position, values of $\underset{\sim}{\xi}$ are given on three other times. These are the present time level t, the previous time level $t - \Delta t$ and the time level of front passage $t - \Delta t_f$ where $\Delta t_f = \|\Delta\tilde{x}\|/\bar{v}_x$ with $\bar{v}_x$ the front passage velocity. This gives three possibilities to determine an estimate for the label set $\underset{\sim}{\xi}(\tilde{x} - \Delta\tilde{x},t - \Delta t')$ (see Fig. 6):

$$\underset{\sim}{\xi}(\tilde{x} - \Delta\tilde{x},t - \Delta t') = \underset{\sim}{\xi}(\tilde{x} - \Delta\tilde{x},t - \Delta t) - \frac{\Delta t' - \Delta t}{\Delta t_f - \Delta t} \times [\underset{\sim}{\xi}(\tilde{x} - \Delta\tilde{x},t - \Delta t) - \underset{\sim}{\xi}(\tilde{x} - \Delta\tilde{x},t - \Delta t_f)], \tag{14}$$

$$\underset{\sim}{\xi}(\tilde{x} - \Delta\tilde{x},t - \Delta t') = \underset{\sim}{\xi}(\tilde{x} - \Delta\tilde{x},t) - \frac{\Delta t'}{\Delta t}[\underset{\sim}{\xi}(\tilde{x} - \Delta\tilde{x},t) - \underset{\sim}{\xi}(\tilde{x} - \Delta\tilde{x},t - \Delta t)], \tag{15}$$

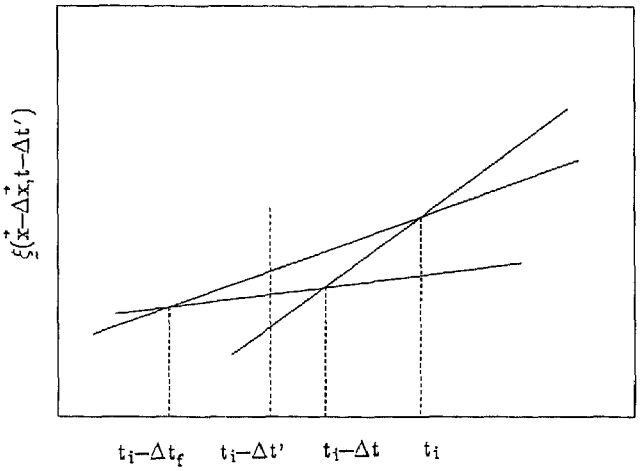

Fig. 6. Three possibilities for the estimation of the label set $\underset{\sim}{\xi}(\tilde{x} - \Delta\tilde{x},t - \Delta t')$

$$\underset{\sim}{\xi}(\tilde{x} - \Delta\tilde{x},t - \Delta t') = \underset{\sim}{\xi}(\tilde{x} - \Delta\tilde{x},t) - \frac{\Delta t'}{\Delta t_f}[\underset{\sim}{\xi}(\tilde{x} - \Delta\tilde{x},t) - \underset{\sim}{\xi}(\tilde{x} - \Delta\tilde{x},t - \Delta t_f)]. \tag{16}$$

Scheme (16) was chosen as, after some numerical experiments, it showed the best results.

5 Application of the front model with temperature and conversion

Important starting-points of the analytical flow front model are isothermal flow and Newtonian material behaviour. As indicated above, it is assumed that, in spite of these simplifications the velocity field is approximated quite well and changes in temperature and conversion field are not of significant influence. For the flow front domain, the energy and the conversion equation can be written in dimensionless form as:

$$Gz\,\varrho^*c_p^*\dot{T}^* = \frac{\partial}{\partial\tilde{x}^*}\left(\lambda^*\frac{\partial T^*}{\partial\tilde{x}^*}\right) + Br\,\eta^*\dot{\gamma}^{*2} - \frac{Br}{Ga}\dot{p}_0^* + DaIV\,\varrho R_c^*, \tag{17}$$

$$\dot{C}^* = DaI\,R_c^*. \tag{18}$$

For typical values for the material parameters and the process characteristics occurring in injection moulding, the Graetz and Damköhler IV number are large, certainly at the flow front. Thus, the energy equation (17) can be rewritten as:

$$Gz\,\Phi^*c_p^*\dot{T}^* = DaIV\,\varrho R_c^*. \tag{19}$$

This implies that in the flow front domain material particles are considered to experience an adiabatic thermal history. For each particle entering the flow front domain temperature and conversion are given and so it is a relatively simple task to compute, by means of numerical integration given the known residence time, the temperature and conversion

of a particle as it leaves the flow front domain, i.e. the particles on gridpoints between folding points and wall.

For particles that enter the flow front domain, i.e. particles on gridpoints between the folding points, the same arguments hold and therefore they are treated similarly.

6 Results

6.1 Cavity with a restriction

To test the influence of mesh coarseness, the filling of a flat cavity with a restriction is simulated. The injected material is a thermosetting material (PU RIM system, [25], see Table 1 for specifications). The viscosity as a function of the temperature T and the conversion $X = C/C_0 - 1$ is given by:

$$\eta(T,C) = A_\eta \exp(E_\eta/RT) \left[\frac{X_{gel}}{X_{gel} - X}\right]^{(A+BX)}, \qquad (20)$$

Second order kinetics with an Arrhenius temperature dependence [15] was used to describe conversion. This material was used in other test cases where the reaction played an important role. In this example the influence of the conversion is minor, however, mainly due to the short filling time. One half of the cavity locally has a finer mesh. This refinement is chosen in the area where one may expect large gradients in the particle paths (see Figs. 7 and 8). The results are only considered with respect to the midplane. Labels refering to the position of injection (Figs. 7a to c) and to the time of injection (Figs. 8a to c) are considered and are given for filling stages of 60, 80 and 100 %.

Table 1. Specification of the PU RIM system used

$c_p = 1880$ J/kg K $\varrho = 1000$ kg/m^3 $C_0 = 2.6e3$ mol/m^3 $A_\eta = 4.1e-8$ Pa · s $k_1 = 9.36e7$ 1/s $A = 4$	$\lambda = 0.17$ W/m K $h_r = 83$ kJ/mol $X_{gel} = 0.85$ $E_\eta = 38.3$ kJ/mol $k_2 = 0$ 1/s $B = -2$
Processing conditions $T_{wall} = 343$ K $t_{fill} = 2$ s $T_{inj} = 327$ K	
Overall dimensions Cavity with restriction: T-shaped cavity:	 $100 \times 200 \times 2$ mm^3 $80 \times 200 \times 2$ mm^3

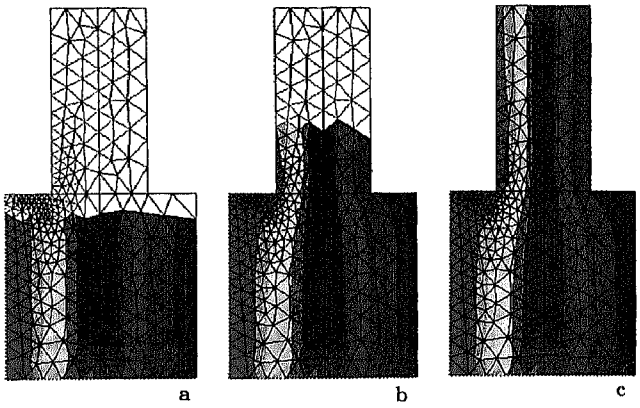

Fig. 7. Distribution of x-labels (injection position) in the midplane of the mould for filling stages of 60 % (a), 80 % (b) and 100 % (c)

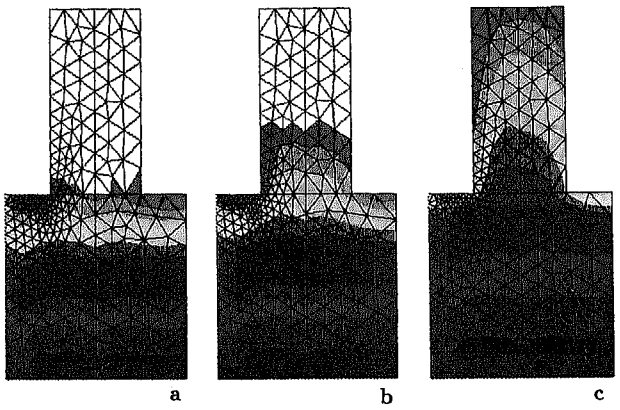

Fig. 8. Distribution of time labels (moment of entering) in the midplane of the mould for filling stages of 60 % (a), 80 % (b) and 100 % (c)

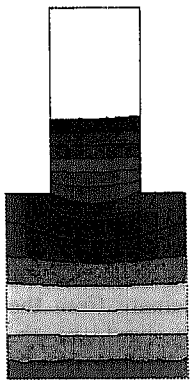

Fig. 9. Contour levels of pressure for a filling stage of 80 %

The influence of the finer mesh is clearly demonstrated. The finer mesh at the left side of the cavity, in the region of transition from a wide to narrow cavity, allows the material that is entered at the side wall to pass along the sharp corner. The reason is a better description of the pressure gradient (see Fig. 9) which dictates the velocity field and thus the particle tracking. This example shows clearly that proper particle tracking requires mesh refinement on different places as prediction of filling patterns does.

6.2 T-shaped cavity

To show the capabilities of the method the filling of a T-shaped cavity, with the same material and processing conditions as in the first example (see Table 1), was simulated. Again, results will only be considered with respect to particle tracking in the midplane of the cavity, although similar results could be given at any arbitrary plane. They are given for 60, 80, and 100 % filling.

Figs. 10a to c show the distribution of the label values that identifies the position where the particle entered the

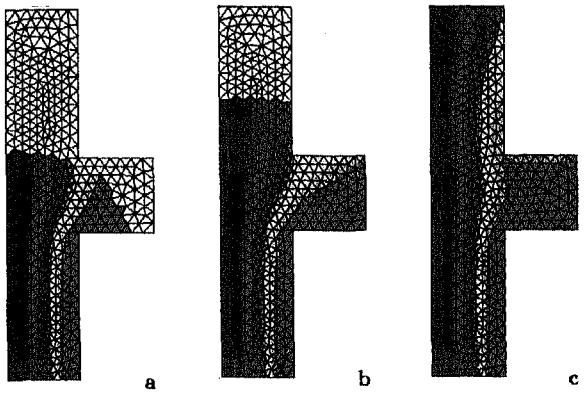

Fig. 10. Distribution of x-labels (injection position) in the midplane of the mould for filling stages of 60 % (a), 80 % (b) and 100 % (c)

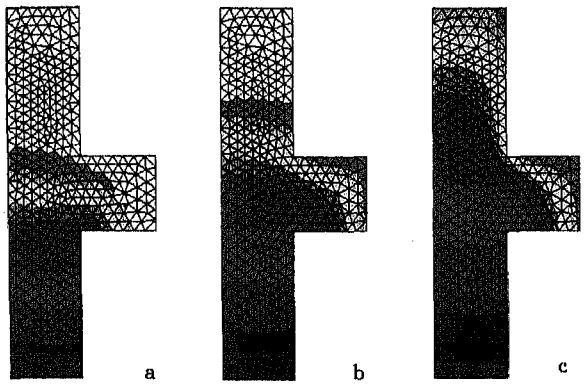

Fig. 11. Distribution of time labels (moment of entering) in the midplane of the mould for filling stages of 60 % (a), 80 % (b) and 100 % (c)

mould. Notice that after the side part of the mould is filled, some material in this part (the yellow) is replaced by new material (red). Apparently, the side part of the cavity is partially washed out.

Figs. 11a to c show the distribution of the label values that identifies the time of injection, and thus the residence time, of a particle in the mould ($\xi_2 = t_r = t_{fill} - t$). Notice that the label values at the front decrease since the material is continuously replaced by "younger" material that flows through the core to the front.

6.3 Sequential two component moulding

Finally, the method was tested by comparing numerical and experimental results using two components, injected sequentially. The product was a flat plate with four ribs. Two ribs are relatively thick compared to the others (Fig. 12). Two components (the same material, a semi-crystalline Polyamide (Zytel 101 L NC-10 from Du Pont) but with different colours) are injected sequentially. The second component is injected after filling 56 % of the cavity. The viscosity is described with a truncated power law model:

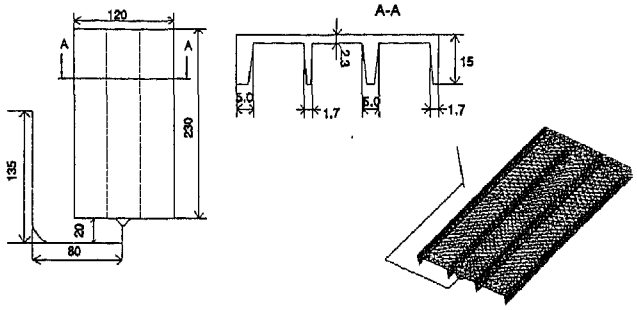

Fig. 12. The testgeometry: a plate with four ribs; two ribs are relatively thick compared to the others

Table 2. Specification of the PA system used

$c_{psol} = 2897$ J/kg K $\lambda_{sol} = 0.1346$ W/m K $m_0 = 34550$ Pa · s $n = 0.61$ $\varrho = 950$ kg/m^3	$c_{pliq} = 2897$ J/kg K $\lambda_{liq} = 0.1346$ W/m K $\varphi = 0.347$ s $\beta = 0.0175$ 1/K

$$\eta(T) = m_0 \exp(-\beta T/n)\varphi^{n-1}, \quad \dot{\gamma} \leq \exp(\beta T/n)\varphi^{-1}, \qquad (21)$$

$$\eta(\dot{\gamma},T) = m_0 \exp(-\beta T)\dot{\gamma}^{n-1}, \quad \dot{\gamma} > \exp(\beta T/n)\varphi^{-1}. \qquad (22)$$

Material parameters are given in Table 2.

The residence time in the mould, one of the labels of the material particles, is used to track the second component. If the residence time is smaller than the time of injection of the second component, the material particle belongs to the first injected component; otherwise to the second component. In each position in the cavity the fraction of the second component, defined over the height of the cavity, is determined.

Figs. 13a to b show the flow front after 77 % filling. The solid line represents the experimentally determined flow

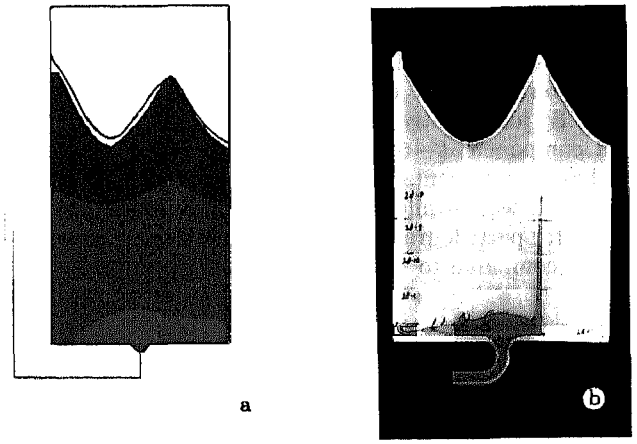

Fig. 13. Position of the flow front for the filling stage of 77 %; comparison of numerical (a) and experimental (b) results

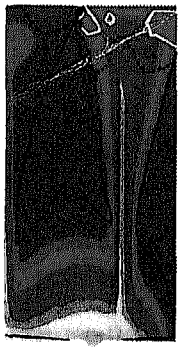

Fig. 14. Numerically determined distribution of the second component injected at a filling stage of 56 %

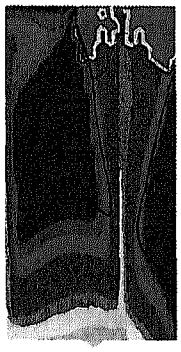

Fig. 15. Numerically determined distribution of the second component injected at a filling stage of 50 %

front. The agreement between experiment and model predictions is satisfactory. In Fig. 14 the distribution of the second component is given in terms of its fraction. The solid line respresents the edge to where the second component has advanced during the experiment. The dashed line indicates the areas where the second component has broken through the first one and is found at the outside of the product. The red areas are the break-through areas as predicted by the numerical simulation. Taking in mind the complex shape and uncertainties in, for example, the thermal boundary conditions and precise experimental conditions, the results can be conceived as good (compared with Fig. 16). By just slightly changing the start of injecting the second component (−6 %) the resemblance between numerical and experimental results is strikingly good (Figs. 15 and 16). It is worthwhile to notice that the extra computation time for particle tracking for the examples presented is negligible compared to the total computation time.

7 Conclusions

Particle tracking by means of labels combined with an analytical model for the flow in the flow front domain were implemented in an existing software program for simulation of injection molding of thin-walled products [1, 2]. This extra task did not cause an appreciable increase in the

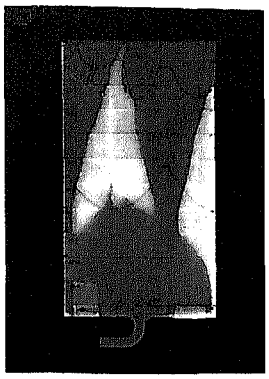

Fig. 16. Experimental distribution of the second component injected at a filling stage of 56 %

computing time. The usefulness of the method is demonstrated and tested. An important aspect proved to be mesh refinement at locations where large gradients in particle paths may be expected. Numerical and experimental results are in good agreement. It is shown that numerical simulations provide a valuable tool for the prediction of particle paths of the complex transient non-isothermal, non-Newtonian flow during injection moulding of (reactive) polymers. Thus, the opportunity exists to predict how to control the sequential and/or simultaneous injection sequence in multilayer injection moulding, even in complex geometries, if recently developed computer codes for the simulation of the injection phase are used [3 to 5].

Future research is aimed at increasing the accuracy through application of more advanced numerical methods such as the van Leer Finite Difference Scheme or the equivalence in finite element methods, the Taylor-Galerkin Discontinuous Finite Element Method (TG/DFEM) [18]. With an improved accuracy, extending of the simulations to multi-component injection moulding with different materials and inversion of the total flow problem can be done with more confidence [19]. The last target aims at the final application, i.e. the inverse problem: once the desired positions of the different materials in the final product are fixed (according to the product design) the numerical simulation will indicate when and where every material particle has to be injected. The development of a flexible valve system is part of this research.

References

1 *Vos, E., Meijer, H. E. H., Peters, G. W. M.:* Multilayer Injection Moulding. Part 1: The Piston driven flow. Int. Polym. Process. 6, p. 1 (1991)
2 *v. d. Velden, P. J. L.:* Particle Tracking in Reactive Flows, Master Thesis (in Dutch), Eindhoven University of Technology, Eindhoven, the Netherlands, 1991
3 *Boshouwers, A. H. M., van der Werf, J. J.:* INJECT-3, A Simulation Code for the Filling Stage of the Injection Moulding Process of Thermoplastics. PhD Thesis, Eindhoven, University of Technology, Eindhoven, the Netherlands, 1988
4 *Douven, L. F. A:* Towards the Computation of Properties of Injection Moulded Products. PhD Thesis, Eindhoven, University of Technology, Eindhoven, the Netherlands, 1991

5 *Sitters, C. W. M.:* Numerical Simulation of Injection Moulding. PhD Thesis, Eindhoven, University of Technology, Eindhoven, the Netherlands, 1988
6 *Isayev, A. I.* (Ed.): Injection and Compression Moulding Fundamentals. Marcel Dekker Inc., New York, 1987
7 *Hieber, C. A., Shen, S. F.:* J. Non-Newtonian Fluid Mech. 7, p. 1 (1980)
8 *Spoelstra, A. B.:* Transfer Moulding of Reactive Materials: Application to the Encapsulation of Integrated Circuits. Designers' Course Computational Mechanics, (WFW92.098), Eindhoven University of Technology, Eindhoven, Sept. 1992
9 *Baayens, F. P. T., Douven, L. F. A.:* Calculation of Flow Induced Residual Stresses in Injection Moulded Products, in *Dijksman, J. F., Nieuwstadt, F. T. M.* (Eds.): Integration of Theory and Applications in Applied Mechanics. Kluwer Academic Publishers, Dordrecht, 1990
10 *Press, W. H., Flannery, B. P., Saul, T., Vettering, W. T.:* Numerical Recipes, Cambridge University Press, Cambridge, 1986
11 *Garcia, A. C.:* Reactive Mold Filling Modeling. PhD Thesis, University of Minnesota, 1991
12 *Kamal, M. R., Goyal, S. K., Chu, E.:* AIChE J. 34, p. 1 (1988)
13 *Garcia, A. C., Macosko, C. W., Subbiah, S., Güçeri, S. I.:* Int. Polym. Process. 6, p. 1 (1991)
14 *Manas-Zloczower, I., Blake, J. W., Macosko, C. W.:* Polym. Eng. & Sci. 27, p. 16, Sept. (1987)
15 *Castro, J. M., Macosko, C. W.:* AIChE J. 28, p. 250 (1982)
16 *Schoone, P.:* Results of the Implementation of Fountain Flow Approximations in Inject-3T. Philips, CFT-Technology 90.15.157, 1990
17 *Coyle, D. J., Blake, J. W., Macosko, C. W.:* AIChE J. 33, p. 7, July (1987)
18 *Johnson, C.:* Numerical Solution of Partial Differential Equations by the Finite Element Method. Cambridge University Press, Cambridge, 1990
19 *Zoetelief, W. F.:* On the Numerical Simulation of the Multilayer Injection Moulding Process. Designers' Course Computational Mechanics, (WFW92.100), Eindhoven University of Technology, Eindhoven, Sept. 1992

Acknowledgement

This research was sponsored by the European Community in the Brite Eurom project Breu-495 BE-4076.

Date received: February 11, 1993
Date accepted: February 18, 1994

Nomenclature

c_p	heat capacity at constant pressure
C	concentration of reactive species
D	diffusion coefficient
H	cavity thickness
h_r	specific reaction heat
p	pressure
R_c	conversion rate
t_r	characteristic reaction time
T	temperature
$\vec{v}$	velocity
V	characteristic velocity
X	extent of reaction (conversion) $= C/C_0 - 1$
η	viscosity
ϱ	density
λ	thermal conductivity
ξ	particle labels
$\vec{\nabla}$	gradient operator

Dimensionless numbers

Brinkman $\quad Br = \dfrac{\eta_0 V^2}{\lambda_0 \Delta T}$

Damkohler I $\quad DaI = \dfrac{H}{V}\dfrac{1}{t_r}$

Damkohler II $\quad \dfrac{H^2}{D}\dfrac{1}{t_r}$

Damkohler IV $\quad DaIV = \dfrac{H\varrho_0 h_r}{\lambda_0 \Delta T t_r}$

Graetz $\quad Gz = \dfrac{\varrho_0}{\lambda_0 c_p}\dfrac{H^2 V}{L}$